

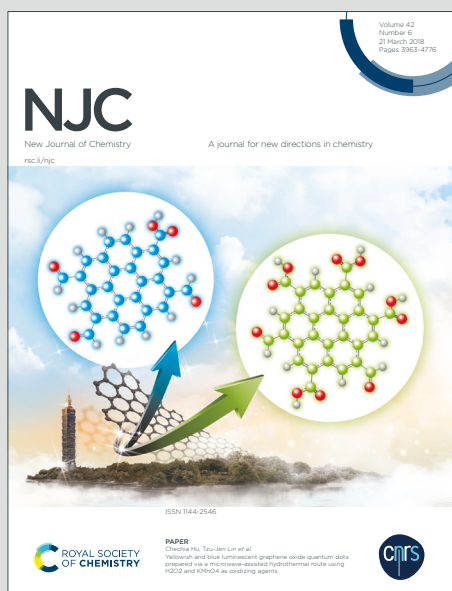
NJC

New Journal of Chemistry

Accepted Manuscript

A journal for new directions in chemistry

This article can be cited before page numbers have been issued, to do this please use: T. Dube, P. Prasad, C. S. Kumar, M. Banerjee and M. Ramteke, *New J. Chem.*, 2025, DOI: 10.1039/D5NJ02091C.



This is an Accepted Manuscript, which has been through the Royal Society of Chemistry peer review process and has been accepted for publication.

Accepted Manuscripts are published online shortly after acceptance, before technical editing, formatting and proof reading. Using this free service, authors can make their results available to the community, in citable form, before we publish the edited article. We will replace this Accepted Manuscript with the edited and formatted Advance Article as soon as it is available.

You can find more information about Accepted Manuscripts in the [Information for Authors](#).

Please note that technical editing may introduce minor changes to the text and/or graphics, which may alter content. The journal's standard [Terms & Conditions](#) and the [Ethical guidelines](#) still apply. In no event shall the Royal Society of Chemistry be held responsible for any errors or omissions in this Accepted Manuscript or any consequences arising from the use of any information it contains.

Beyond Immune Escape in SARS-CoV-2: An ACE2 Functionalized Gold Nanoparticle Vertical Flow Assay for Saliva-Based Detection

View Article Online
DOI: 10.1039/C3NJ02091C

Tejal Dube¹, Puja Prasad^{1,2}, Chandra Shekhar Kumar³, Manidipa Banerjee³ and Manojkumar Ramteke^{1*}

¹Department of Chemical Engineering, Indian Institute of Technology Delhi, 110016, India

²Amity Institute of Click Chemistry Research and Studies, Amity University, Noida, Uttar Pradesh 201303, India

³Kusuma School of Biological Sciences, Indian Institute of Technology Delhi, Hauz Khas, New Delhi 110016, India

*Corresponding author: mcramteke@chemical.iitd.ac.in

Abstract

Rapid and accurate detection of SARS-CoV-2 is crucial as the spread of COVID-19 has reported more than 5.4 million deaths worldwide, causing the pandemic. SARS-CoV-2, being an RNA virus, is prone to mutations over time. A point mutation in RNA can lead to structural variations in the spike protein, the primary target of vaccines and immune responses. This can make the virus less recognizable to antibodies generated from previous infections or vaccinations. In this study, we present a novel flow-through assay for the detection of SARS-CoV-2 in saliva targeting conserved regions of the viral spike protein. The designed assay includes angiotensin-converting enzyme 2 (ACE 2) functionalized gold-nanoparticles (AuNPs) for viral capture and signalling platform. ACE 2 is the key receptor for the spike protein, offering a precise binding mechanism. Also, the use of saliva makes the test more user-friendly, preventing false results arising from incorrect and inadequate sample collection. The viral capture by ACE2 leads to changes in the optical properties of the AuNPs, causing the visual color change. The characterization of specialized nanoparticles was done by UV spectroscopy, Dynamic light scattering, Zeta potential, and Transmission Electron Microscopy. This assay demonstrates high sensitivity and specificity of 96.67% and 95% respectively, with Area under the Curve of 0.99. The LoD of 0.02 pg/ μ l is comparable to standard PCR tests with significantly reduced processing time. Moreover, the kit outperformed the saliva-based marketed LFA-kit when tested for 30 spiked samples. The simplicity of the developed flow-through design enables point-of-care applicability, preventing future outbreaks.

Keywords: SARS-CoV-2, ACE2, gold nanoparticles, saliva, flow-through assay, rapid detection, COVID-19 diagnostics

Introduction

The global outbreak of SARS-CoV-2 has underscored the urgent need for rapid, sensitive, and scalable diagnostic platforms. The World Health Organization (WHO) has extensively documented the global impact of SARS-CoV-2 since the onset of the COVID-19 pandemic.

SARS-CoV-2, like all RNA viruses, is highly prone to mutations, which can significantly impact its transmissibility, immune evasion, and detection ¹. Even a single point mutation in the viral genome can lead to structural changes in the spike (S) protein, the primary target of both vaccines and immune responses ². These alterations can reduce the ability to neutralize antibodies generated from prior infections or vaccinations, potentially leading to breakthrough infections and reinfections ³. The continuous evolution of SARS-CoV-2 demands that diagnostic strategies be designed to remain effective against emerging variants. Traditional RT-PCR remains a highly sensitive method for viral detection, but it can become less effective when significant mutations occur in the viral genome, particularly in the targeted regions of the primers and probes ⁴. Therefore, a critical approach in diagnostic development is targeting conserved regions of the spike protein rather than rapidly mutating epitopes. By focusing on conserved regions of the virus, biosensors can maintain high sensitivity and specificity even as new variants emerge. Additionally, integrating advanced materials such as graphene (Sadique et al., 2022; Zaccariotto et al., 2021), gold nanoparticles (Ahmed et al., 2016), and carbon nanotubes (Bardhan et al., 2021) enhances signal transduction, improving detection limits for early-stage infections ⁵. The low detection limits of biosensors ensure accurate detection even at lower viral loads, enabling timely isolation and treatment before widespread transmission reoccurs.

Beyond the current landscape of SARS-CoV-2, the development of diagnostic kits targeting conserved viral regions is essential for future outbreak preparedness. Such an approach ensures adaptability for detecting novel variants and even related coronaviruses that may pose future pandemic threats like SARS-CoV-1 (2003 outbreak), MERS, and common cold coronaviruses (HCoV-OC43, HCoV-HKU1, etc.), RSV, and paramyxoviruses ⁶. As COVID-19 transitions into an endemic phase, these next-generation diagnostics will play a crucial role in continuous surveillance, variant monitoring, and rapid response to emerging infectious diseases.

Detection of SARS-CoV-2 in saliva has proven to be comparable to, and in some cases more advantageous than nasopharyngeal swabs. It provides advantages due to its non-invasive nature and ease of sample collection ⁷. Saliva-based testing minimizes the discomfort and risks associated with nasopharyngeal swabs, such as patient-induced coughing or sneezing during collection ⁸. Studies have demonstrated similar sensitivity and specificity between the two methods, providing evidence of saliva as a reliable diagnostic alternative ⁹. A few studies reported in the literature show evidence of its potential. A study reported ¹⁰ employs graphene-based field-effect transistor (FET) biosensors for label-free virus detection, leveraging

1
2
3 advanced nanomaterials for enhanced sensitivity. Meanwhile, another study introduces an View Article Online
DOI: 10.1039/D3NJ02091C
4 electrochemical biosensor with single-walled carbon nanotubes and gold nanoparticles for
5 nucleocapsid protein detection ⁸. In contrast, ¹¹ and ¹² focus on saliva as a diagnostic sample;
6 the former highlights the RT-LAMP method for cost-effective and rapid detection. While the
7 latter underscores saliva's non-invasive nature and reliability compared to nasopharyngeal
8 swabs. Further study ¹³ explores a colorimetric biosensor using gold nanoparticles for RNA
9 detection, enabling easy visual readouts, whereas ¹⁴ introduces a plasmonic photothermal
10 biosensor combining optical and thermal detection mechanisms. Finally, ¹⁵ evaluates clinical
11 diagnostic methods focusing on laboratory-based RT-PCR for sensitivity and accuracy.
12 Collectively, these studies illustrate a diverse range of technologies, sample types, and
13 detection principles, showcasing the multifaceted nature of SARS-CoV-2 diagnostic research.

14
15
16
17
18
19
20
21
22
23
24
25
26
27
28
29
30
31
32
33
34
35
36
37
38
39
40
41
42
43
44
45
46
47
48
49
50
51
52
53
54
55
56
57
58
59
60
Although working with real viral samples can be dangerous and life-threatening. To overcome
this limitation, virus-like particles (VLPs) that mimic the structure of SARS-CoV-2 have
emerged as a safe and effective tool for diagnostic research and assay development. VLPs lack
the viral genome, rendering them non-infectious. However, they retain the key structural
proteins, including the spike protein, enabling them to interact specifically with the ACE2
receptor ¹⁶. By exploiting this interaction, novel biosensor platforms are being developed to
achieve rapid and accurate detection of SARS-CoV-2 VLPs ¹⁷ ¹⁸. On the other hand, gold
nanoparticles (AuNPs) have proven to be highly effective in biosensing applications due to
their unique optical properties, high surface-area-to-volume ratio, and ease of functionalization
¹⁹. When conjugated with ACE2 receptors, AuNPs enable specific binding to SARS-CoV-2
VLPs, thereby enhancing both detection sensitivity and specificity. Integrating these
functionalized nanoparticles into a flow-through assay format offers additional advantages,
which include reduced assay time, minimal sample handling, and the potential for high-
throughput applications ²⁰. Most SARS-CoV-2 diagnostic techniques rely on sandwich assays
using antibodies, but these have significant limitations. Antibody-based assays are prone to
reduced sensitivity when viral mutations alter the antigen structure, leading to false negatives
²¹. Additionally, antibodies can exhibit cross-reactivity, causing false positives with other
coronaviruses. Production of high-affinity antibodies is costly, time-consuming, and subject to
batch-to-batch variability ²². In contrast, very few techniques directly target the antigen, rather
have shown the detection of host-generated antibodies, which also have drawbacks. Antibody
detection is ineffective for early diagnosis, cannot differentiate between past and active
infection, and is influenced by declining immunity, limiting its diagnostic reliability ^{23,24}.

1
2
3 Additionally, incapable of detecting the immune escape variants ²¹. After understanding the
4 demerits of the reported and existing techniques, we have tried to address them in our study. View Article Online
DOI: 10.1039/C5NJ02091C

5
6
7 Therefore, in this study, we report the development of a rapid flow-through assay for the
8 detection of SARS-CoV-2 virus-like particles (VLPs) using the nitrocellulose membrane
9 cassette in saliva using gold nanoparticle-ACE2 receptor functionalization (**Fig. 1b**). The assay
10 exploits the high affinity between the conserved regions of the spike (S1) protein and the ACE2
11 receptor to achieve specific and sensitive detection without the use of additional antibodies or
12 probes (**Fig. 1a**). The incorporation of AuNPs enhances signal readout by observing the color
13 change. Additionally, the developed assay performance is compared to the marketed Angcard
14 saliva-based LFA kit to analyze its potential in large-scale screening. By leveraging the flow-
15 through format, this platform offers significant advantages in terms of speed, ease of use, and
16 adaptability to high-throughput screening. The integration of saliva as the primary sample
17 matrix further enhances the assay's practicality for non-invasive and large-scale testing.
18
19
20
21
22
23
24
25
26
27
28
29
30
31
32
33
34
35
36
37
38
39
40
41
42
43
44
45
46
47
48
49
50
51
52
53
54
55
56
57
58
59
60

Materials and Methods

Reagents.

Gold(III) chloride trihydrate ($\text{HAuCl}_4 \cdot 3\text{H}_2\text{O}$), Uranyl acetate, 1-ethyl-3-(3-dimethylaminopropyl) carbodiimide (EDC), N-hydroxysuccinimide (NHS) Sigma Aldrich (India), ethylenediaminetetraacetic acid (EDTA), SARS co-Virus Like Particles (VLPs) sodium citrate dihydrate ($\text{C}_6\text{H}_5\text{Na}_3\text{O}_7 \cdot 2\text{H}_2\text{O}$), sodium chloride (NaCl), bovine serum albumin (BSA), ACE-2 receptor (Sigma-Aldrich), spike-1 protein (Sigma-Aldrich), and 4-(2-hydroxyethyl)-1-piperazineethanesulfonic acid (HEPES) were from Sigma-Aldrich (India). This study also used carboxythiol-polyethylene glycol (CT-PEG) linker (MW, 634.77 Da) from Fisher Scientific (India), absolute ethanol (EMSURE; Merck, Germany), Nitrocellulose membranes (CX-1, SCNM-I), and absorbent pads (type-AP080) (Advanced Micro Devices Pvt. Ltd., India), saliva-based test kit (Angcard). All other standard reagents used were of analytical grade. All solutions were prepared using ultrapure deionized Milli-Q water ($\sim 18.8 \text{ m}\Omega\text{cm}$ resistivity, CDUFB1001; Millipore, USA). Due to the known pyrogenicity and toxicity of Uranyl acetate, strict safety guidelines were followed in the laboratory while handling these molecules (17).

Methods.

Synthesis of AuNPs conjugates

Gold nanoparticles (AuNPs) with an approximate diameter of 16 nm (AuNP-ACE2-1) and 40 nm (AuNP-ACE2-2) were synthesized using the Turkevich method, as described in previous studies²⁵. Briefly, 5 mg of 0.01% w/v gold (III) chloride (HAuCl₄) was dissolved in 39 mL of deionized (DI) water. Simultaneously, a reducing solution was prepared by combining 2 mL of 1% w/v trisodium citrate with 8 mL of DI water. The gold precursor solution was then heated to its boiling point under continuous stirring, at which point, 1 ml of reducing solution was introduced dropwise, a critical step in the synthesis process. The reaction was allowed to proceed until the solution developed a characteristic wine-red color, indicative of AuNP formation. The resulting nanoparticle suspension was subsequently quenched in an ice bath and stored at 4 °C for further use.

AuNP-ACE2 particle synthesis

The synthesized AuNPs were aliquoted (1ml) in different glass vials. These synthesized particles were stabilized by carboxythiol-polyethylene glycol (CT-PEG) coating by applying 10 µl of 0.1% w/v to every 1 ml of aliquoted AuNP solution to enhance colloidal stability. Further, these particles were left for overnight incubation in a shaker incubator at 30°C at 125 rpm. After incubation, particles were stepwise centrifuged at 4000 rpm and 6000 rpm for 15 minutes each. Finally, the particles were resuspended in 1 ml of 40 mM HEPES buffer with pH 6.0. The PEGylated AuNPs were then functionalized with the angiotensin-converting enzyme 2 (ACE2) receptor *via* EDC-NHS coupling chemistry. Specifically, 6 µl of 0.2 M EDC was added to 1 mL of the AuNP-PEG coated suspension and incubated for 30 minutes at 30°C. After which, 12 µl of 0.2 M NHS was introduced and allowed to react for 30 minutes at 30°C. After incubation, particles were again stepwise centrifuged at 4000 rpm and 6000 rpm for 15 minutes each. Finally, the particles were resuspended in 1 ml of 40 mM HEPES buffer with pH 7.4. The AuNP-ACE2-1 and AuNP-ACE-2 conjugates were then prepared by adding 1.2 µL and 1.8 µl of ACE2, respectively, from a 0.5 µg/µL stock solution to 1 mL of the AuNP suspension. The functionalized AuNPs were stored at 4 °C and remained stable for at least one week.

Particle characterization

1
2
3 The synthesized solution was characterized using UV-visible spectroscopy (UV-2600; Shimadzu), dynamic light scattering (DLS, Zetasizer Nano ZS90; Malvern Instruments Ltd.),
4
5 and transmission electron microscopy (TEM, Tecnai G2). For TEM analysis, a 4× diluted
6
7 AuNP suspension was deposited onto a carbon-coated copper TEM grid (CF200 CU; Electron
8
9 Microscopy Sciences, USA), air-dried, and imaged at an accelerating voltage of 200 kV.
10
11 Micrographs obtained at different magnifications were analyzed using ImageJ software to
12
13 determine the average particle size. The measurements were repeated three times, and the
14
15 results were reported as the mean ± one standard deviation (SD). Additionally, in the case of
16
17 spike protein, virus-like particles (VLPs) and AuNP-ACE2 conjugates were characterized
18
19 using TEM (JEOL JEM-1400). For this, 10 µL of each sample was deposited onto TEM grids,
20
21 air-dried, and stained with 5 µl of 0.5 % uranyl acetate to enhance contrast and stability.
22
23 Imaging was performed at an accelerating voltage of 120 kV across multiple magnifications.
24
25 Micrographs obtained at different magnifications were analyzed.

UV-Visible titration experiment with spiked protein

26
27 The stock solution (0.99 µg/µl) of spike protein was diluted to 0.33 µg/µl using HEPES buffer.
28
29 The AuNP-ACE2 conjugates were titrated with 1 µl of the above diluted spike protein solution
30
31 and incubated for 2 minutes. The absorbance spectra were recorded after each addition of spike
32
33 protein. The experiment was repeated till there was no further shift observed in the spectra.
34
35

Biological matrix collection and preprocessing

36
37 Approximately 1 mL of self-collected saliva was collected in a 2 mL Eppendorf tube and
38
39 subjected to centrifugation at 3000 rpm for 15 minutes at room temperature. The resulting
40
41 supernatant was carefully collected for subsequent analysis. Similarly, plasma samples
42
43 available in the laboratory were aliquoted into 1 mL portions and centrifuged under the same
44
45 conditions at 3000 rpm for 15 minutes at room temperature. The supernatant was carefully
46
47 separated, avoiding the pellet, and used for further experimentation.
48
49

Preparation of spiked saliva and plasma samples.

50
51 A master stocks of virus-like particles (VLPs) at a concentration of 5.6 µg/µL in VLP storage
52
53 buffer were obtained from the Kusuma School of Biology, IIT Delhi. The VLP storage buffer
54
55 comprised 50 mM HEPES, 100 mM NaCl, and 1 mM EDTA, with the pH adjusted to 7.4. The
56
57 VLPs exhibited a stability period of 72 hours, during which all subsequent experiments were
58
59 conducted. For interaction studies under controlled conditions, a working solution of VLPs at
60

1
2
3 a concentration of 1.4 $\mu\text{g}/\mu\text{L}$ was prepared. A calculated volume of VLP solution was spiked
4 into the required volume of human saliva and plasma to achieve final concentrations ranging
5 from 0.5 ng/mL to 1000 ng/mL. The spiked samples were stored at 4°C until further use. Before
6 analysis, the samples were vortexed using a micropipette for a few minutes at room temperature
7 to ensure homogeneity.
8
9

10 *Flow through assay procedure.*

11
12 A standard flow-through assay was designed using a nitrocellulose membrane positioned atop
13 a set of absorbent pads enclosed within custom-fitted plastic cassettes. The absorbent pads
14 functioned as liquid reservoirs and provided mechanical support for the thin membrane. Before
15 the sample application, the membrane surface was treated with 30 μL of 1% surfactant solution
16 (PF68) and allowed to incubate for 2 minutes. Subsequently, 10 μL of the test sample
17 containing either spike protein or virus-like particles (VLPs) was drop-cast at the center of the
18 membrane, followed by the addition of 40 μL of 1% (w/v) bovine serum albumin (BSA) to
19 minimize nonspecific binding. After another 2-minute incubation, 20 μL of a AuNP-ACE2
20 nanoparticle solution was applied to the membrane. The formation of a distinct pink spot
21 against a white background was indicative of the presence of VLPs in the test sample. Finally,
22 the membrane was washed with 10 μL of VLP buffer to remove any unbound nanoparticles.
23 For the control cassette same procedure was followed; the only variation was that saliva
24 without VLPs spike was used at step 2. The entire assay was conducted under ambient
25 conditions, with a relative humidity of 30% to 70% and a temperature of $30 \pm 5^\circ\text{C}$.
26
27
28
29
30
31
32
33
34
35
36
37
38
39
40
41
42
43
44
45
46
47
48
49
50
51
52
53
54
55
56
57
58
59
60

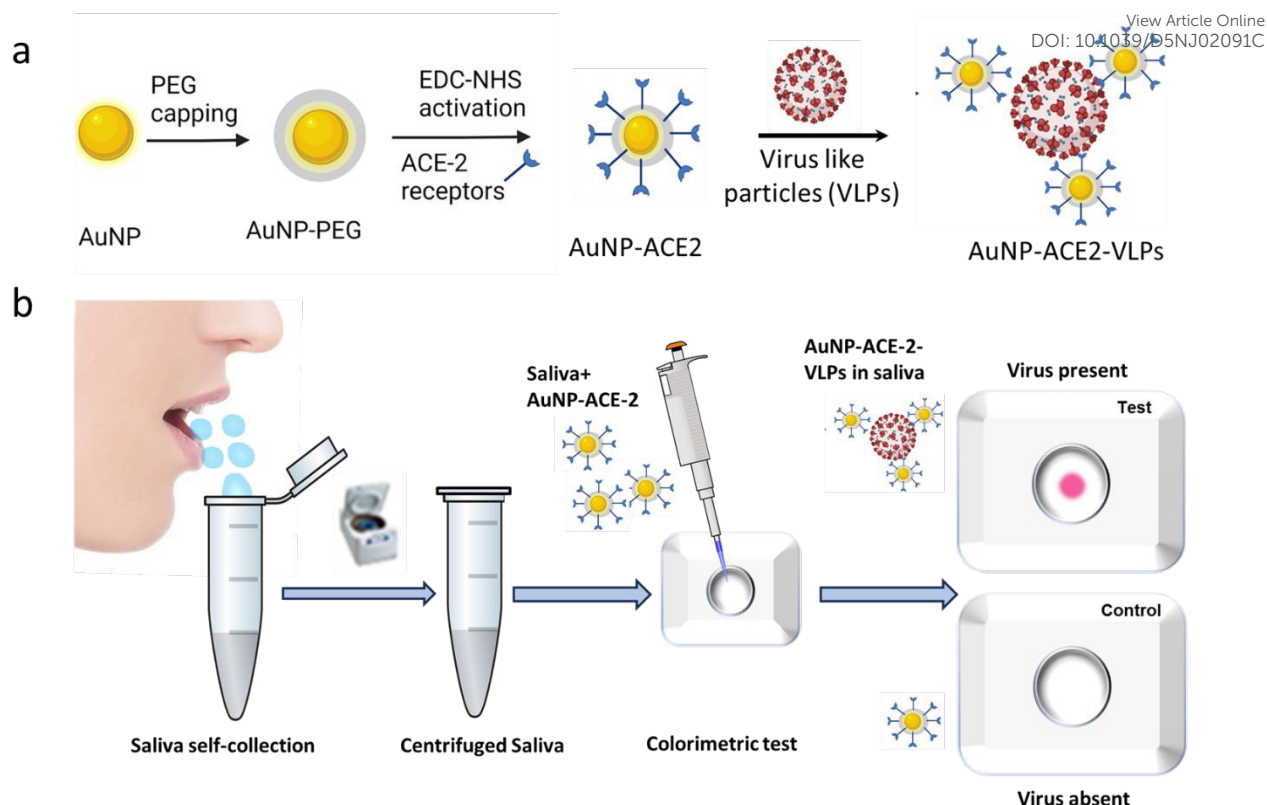


Figure 1: Schematic representation of (a) SARS-CoV-2 VLPs with synthesized AuNP-ACE2 nanoparticles and (b) steps for application on the membrane cassette for stratification of infected individuals.

Results:

Synthesis and characterization of AuNPs-ACE2 particle: Monodisperse gold nanoparticles (AuNPs) have demonstrated exceptional signal amplification and a strong visual colorimetric response, making them widely utilized in various biosensors and point-of-care (POC) diagnostic assays. However, multiple studies have reported the inherent instability of AuNPs, which can lead to rapid aggregation and a color shift from red to purple²⁶. A critical design consideration of the system for its successful implementation was the minimization of nonspecific interactions between AuNPs and the membrane or biological interface. To mitigate this issue, the nanoparticle's surface was passivated using PEG. This modification prevented nonspecific binding by eliminating background signal interference and significantly enhanced nanoparticle stability. PEG capping was employed to maintain monodispersity and prevent undesired aggregation, resulting in nanoparticles that remained stable for several weeks post-synthesis.

Comprehensive characterization of the synthesized AuNP-ACE2 nanoparticles was conducted using UV-vis spectroscopy, dynamic light scattering (DLS), and zeta potential analysis. Transmission electron microscopy (TEM) imaging, followed by size analysis using ImageJ software, confirmed the nanoparticle dimensions to be 34 nm. DLS and zeta potential measurements were consistent with these findings (**Fig. 2**). Conjugation of ACE2 receptors onto the AuNP-PEG surface was achieved using EDC-NHS chemistry, a well-documented approach for stable biomolecular attachment^{27,28}. Successful conjugation was evidenced by a 2 nm and 3 nm red shift in the UV-Vis spectra for **AuNP-ACE2-1** and **AuNP-ACE2-2**, respectively (**Fig. 2a**). The DLS study showed a ~2-fold increase in hydrodynamic particle diameter from 34 nm AuNPs particle size to 54 nm and 62 nm for **AuNP-ACE2-1** and **AuNP-ACE2-2**, respectively confirming successful conjugation of ACE2 receptor on the surface of AuNP nanoparticles (**Fig. 2b**). Additionally, zeta potential analysis showed a clear reduction following PEG capping, which subsequently increased upon ACE2 receptor conjugation (**Fig. 2d**), further confirming successful functionalization. The representative TEM image showing dispersed nanoparticles used for the ACE2 conjugation is provided (**Fig. 2e**). The particle count was done using the TEM data from ImageJ, and there were 45 particles found in the range of 35-40 nm (**Fig.2c**).

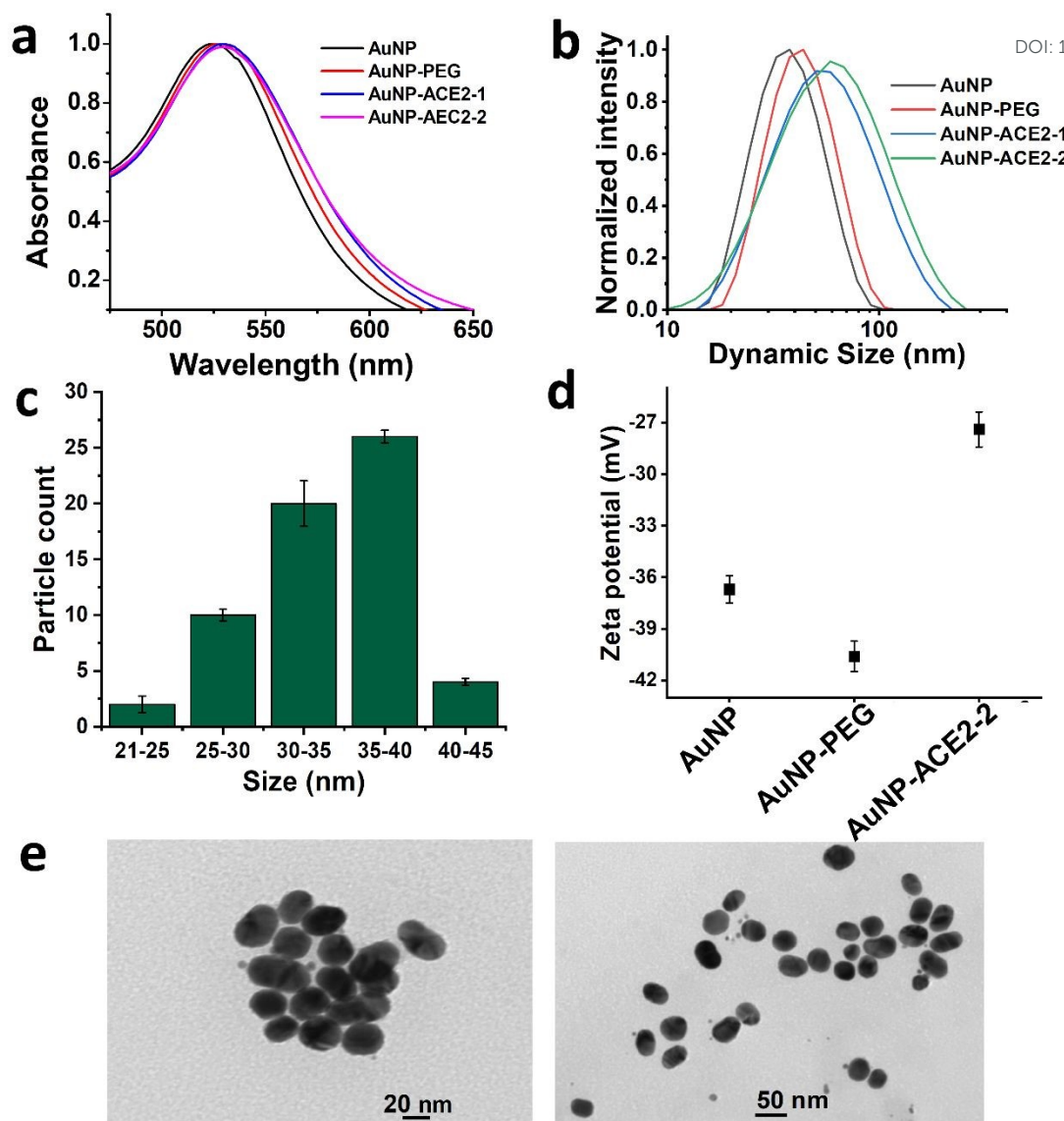


Figure 2: Characterization of gold nanoparticles (AuNPs) and particles coated with ACE2 receptor using EDC-NHS coupling reaction (a) UV-Vis absorbance spectra with a red shift after conjugation with ACE2 receptor, (b) DLS data showing increased hydrodynamic diameter with successful conjugation, (c) particle count of **AuNP-ACE2-2** from TEM imaging data, (d) Zeta potential confirming conjugation of ACE2 receptor with AuNP. (e) TEM images of **AuNP-ACE2-2** at 60000X and 44000X magnification at 20 nm and 50 nm scale bar, and all the data is reported as the average of triplicate readings.

Optimization of membrane: A range of additional parameters were systematically optimized to determine the ideal operating conditions for optimal assay performance (refer to **Table S1** in the supplementary material). Notably, surfactants played a critical role in the immobilization process. The lipid bilayer and membrane proteins impart a degree of

lipophilicity to the VLPs, facilitating interactions with hydrophobic surfaces and enhancing immobilization on the membrane. The inclusion of surfactants improved the wettability of the injected solution. This adjustment ensured an optimal hydrophilic-lipophilic balance, promoting uniform adsorption of the VLPs. Additionally, minimizing nonspecific interactions between AuNPs and the membrane or protein interface in the biological matrix was a key consideration in assay design. Furthermore, to eliminate any surface-related nonspecific binding, the membrane was pre-blocked with a BSA solution (**Fig. S1**)²⁵.

Interaction study of AuNP-ACE2 with spike (S1) protein: Research has demonstrated that the Spike protein of SARS-CoV-2 exhibits a higher binding affinity for the ACE2 receptor compared to that of SARS-CoV²⁹. A strong interaction between the target antigen and its corresponding antibodies or receptor is essential. It enables the development of effective therapeutics, vaccines, and is also essential for designing highly sensitive and accurate diagnostic assays for antigen detection. The spike (S1) protein identified in the literature as the epitope of the virus with the highest reported affinity for the ACE2 receptor, was utilized as a controlled study to investigate and validate its interaction with the synthesized specialized nanoparticles (**Fig. 3a, b**). For this, UV-visible titration studies were conducted using spike S1 protein and synthesized nanoparticle **AuNP-ACE2-1** and **AuNP-ACE2-2**. With addition of 1.32 μg (4 μl) of spike protein, 7 nm of red shift with no visual change in the colour of **AuNP-ACE2-1** was observed upon addition of spike protein (**Fig. 3a**). However, in case of **AuNP-ACE2-2**, red shift of 19 nm of was observed with visual color change from purple to violet upon addition of spike protein. This could be due to the aggregation of **AuNP-ACE2-2** upon the addition of spike protein (**Fig. 3b**). The greater red shift in **AuNP-ACE2-2** demonstrated better binding ability of **AuNP-ACE2-2** with spike protein than **AuNP-ACE2-1**. Further, the interaction of **AuNP-ACE2-2** with spike protein was confirmed by performing the DLS of the synthesized particles after the addition of spike protein to the solutions. The DLS data plotted in **Fig. S2** showed an increase in hydrodynamic diameter by 11 nm, which is suggestive of the successful binding of spike protein to the particle surface by non-covalent bonds, including hydrogen bonds, van der Waals forces, and electrostatic interactions³⁰. Since the final application involved immobilization on a membrane surface, interaction studies were conducted using membrane cassettes to evaluate the formation of a distinct pink spot upon the stepwise sample addition (**Fig. 3c**). For this purpose, AuNP-ACE2 receptor conjugates binding efficiency was analysed with the spike protein, two different spike buffer-to-spike protein ratios (1:1 and 1:4) were evaluated, representing a diluted and a more concentrated condition,

respectively. The optimal visual response was observed with the **AuNP-ACE2-2** suspension which produced a well-defined and distinct pink spot, whereas the **AuNP-ACE2-1** resulted in patchy and faint spots that were difficult for the end user to interpret. However, the visibility of the pink spot remained consistent across both spike protein concentrations (1:1 and 1:4) (Fig.3d).

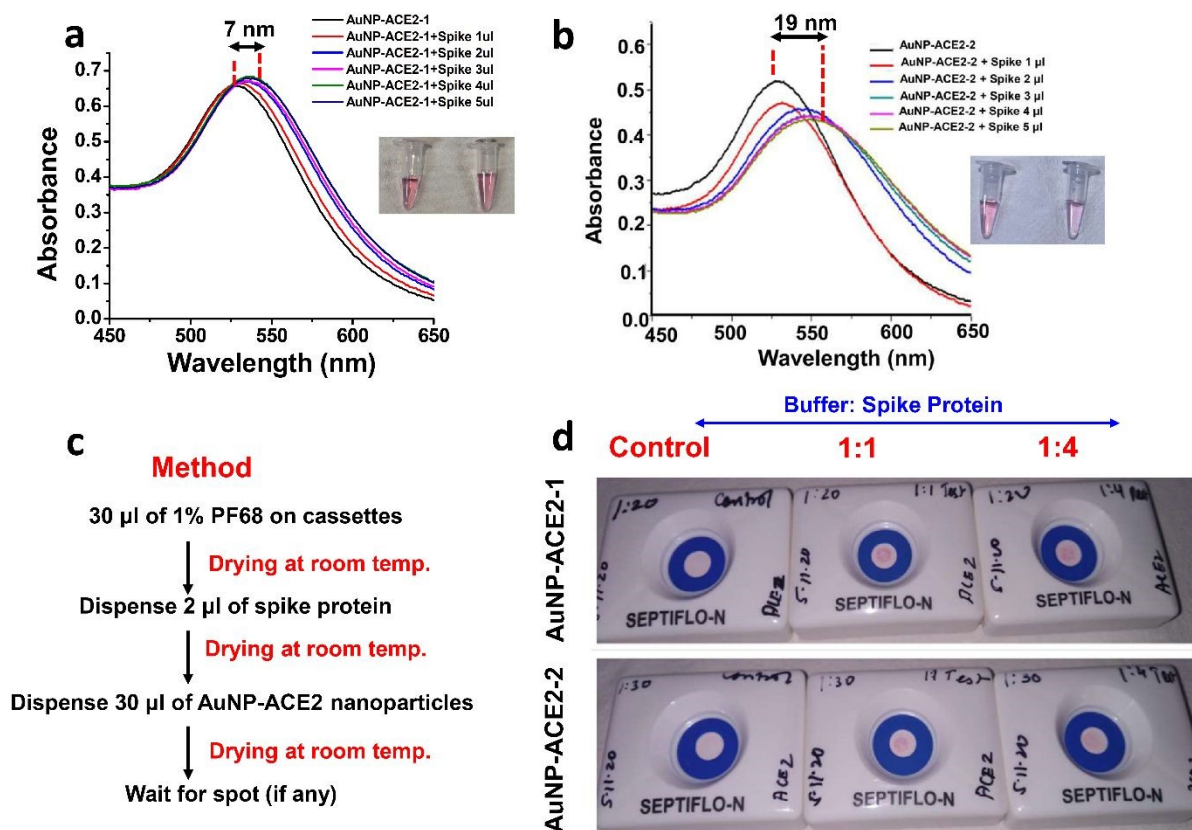


Figure 3: Interaction studies by UV-vis titration with (a) **AuNP-ACE2-1** and (b) **AuNP-ACE2-2** with increasing concentration of S1 spike protein of Sars Covid-19 virus, and (c) study on membrane cassette.

Interaction study of AuNP-ACE2-2 with SARS-CoV-2 VLPs: The amphiphilic nature of VLPs can cause non-specific binding and self-aggregation due to the lipid bilayer membrane³¹. Accomplishing the interaction of nanoparticles with the spike protein present on the surface of *in vitro* synthesized VLPs in a controlled environment is of utmost importance. The interaction of VLPs with AuNP-ACE2-2 particles was investigated using UV-visible spectroscopy, taking VLP buffer and AuNP-PEG (without ACE2 receptor) as controls to identify nonspecific binding and false aggregation. The result showed a decrease in the absorbance intensity at 532 nm when AuNP-ACE2-2 is titrated with VLPs compared to their controls (Fig. 4a). The DLS data recorded the increased hydrodynamic diameter from 55 nm

of AuNP-ACE2-2 to 254 nm, demonstrating successful interaction of AuNP-ACE2-2 with VLPs. This increase in the size could be attributed to multiple VLPs binding to a single particle surface (Fig. 4b). This interaction was also confirmed by TEM imaging as shown in Fig. 4c. The VLPs were consistently verified for their specific interaction with the ACE2-coated AuNPs. Therefore, it can be used for further membrane-based optimization of the assay. The use of antibodies was not found necessary as the ACE2 receptor itself gave specificity without the use of secondary antibodies. This made the assay even more cost-effective.

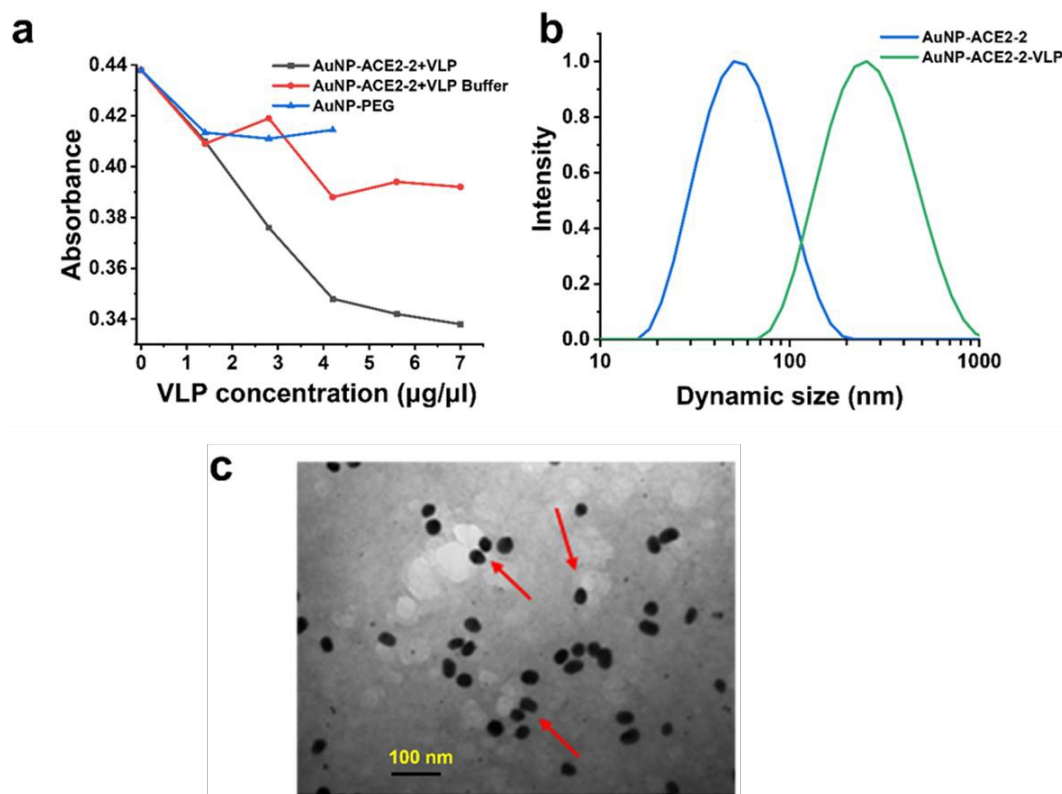


Figure 4: Characterization of the interaction of synthesized AuNP-ACE2-2 with VLPs of Sars Covid-19, (a) UV-vis spectra for increasing concentration of VLPs with AuNP-ACE2, (b) DLS data showing increased hydrodynamic diameter with successful interaction with VLPs (c) representative TEM micrograph taken at 30000X magnification at 100 nm scale bar confirming VLPs capture by synthesized AuNP-ACE2-2 particles at multiple sites denoted in red arrows and a dotted circle.

Performance study in different biological fluids:

To evaluate the performance of the developed assay across different biological matrices, we tested its efficacy in saliva and blood plasma. The performance of AuNP-ACE2-2 nanoparticles was evaluated using UV-visible spectroscopy by titrating VLPs spiked in the biological matrices (saliva or plasma). As a control, the interaction studies were conducted using a biological matrix with VLP storage buffer. The results indicated that the assay exhibited

1
2
3 significantly better performance in the saliva matrix compared to plasma. In plasma, the
4 absorbance intensity of AuNP-ACE2-2 at 532 nm continuously increases in both, control and
5 spiked plasma with VLPs with minimal absorbance variation between them (**Fig.5b**). However,
6 in saliva samples spiked with VLPs demonstrated a distinctly higher absorbance compared to
7 the control (**Fig.5a**). The results also showed the VLPs spiked sample had a higher absorbance
8 consistently with increasing concentration of VLPs whereas the absorbance dropped with
9 increasing buffer concentration in the saliva sample in the respective controls.
10
11
12
13
14
15

16 Furthermore, for more practical applications, we extended the interaction studies between
17 AuNP-ACE2-2 with VLPs spiked in biological matrix from liquid-phase to membrane-based
18 experiments. Membranes serve as highly effective point-of-care (POC) affinity scaffolds. This
19 is due to their tunable surface properties, which allow for receptor-independent immobilization
20 of target molecules, and their adjustable porosity, which enables precise control over fluid
21 dynamics. The term "receptor-independent" refers to the ability of analytes to be directly
22 captured on the membrane surface without the necessity of ligand- or receptor-based
23 interactions, such as those mediated by antibodies. The assay was performed within flow-
24 through membrane cassettes, wherein a drop of VLP-spiked sample in biological matrix (like
25 plasma and saliva) was first introduced, followed by the addition of an AuNP-ACE2
26 suspension. A well-defined visual spot was observed only in the saliva matrix, whereas in
27 plasma, no detectable color gradient was evident when compared with the control cassette (**Fig.**
28 **S3**). Further, the sequentially increasing concentration of VLPs spiked in the saliva developed
29 a very defined visual gradient in the pink spot (**Fig. 5c**) that can be combined with an optical
30 sensor to increase the scope of the assay, not only for qualitative analysis but also towards
31 quantitative analysis.
32
33
34
35
36
37
38
39
40
41
42
43
44
45
46
47
48
49
50
51
52
53
54
55
56
57
58
59
60

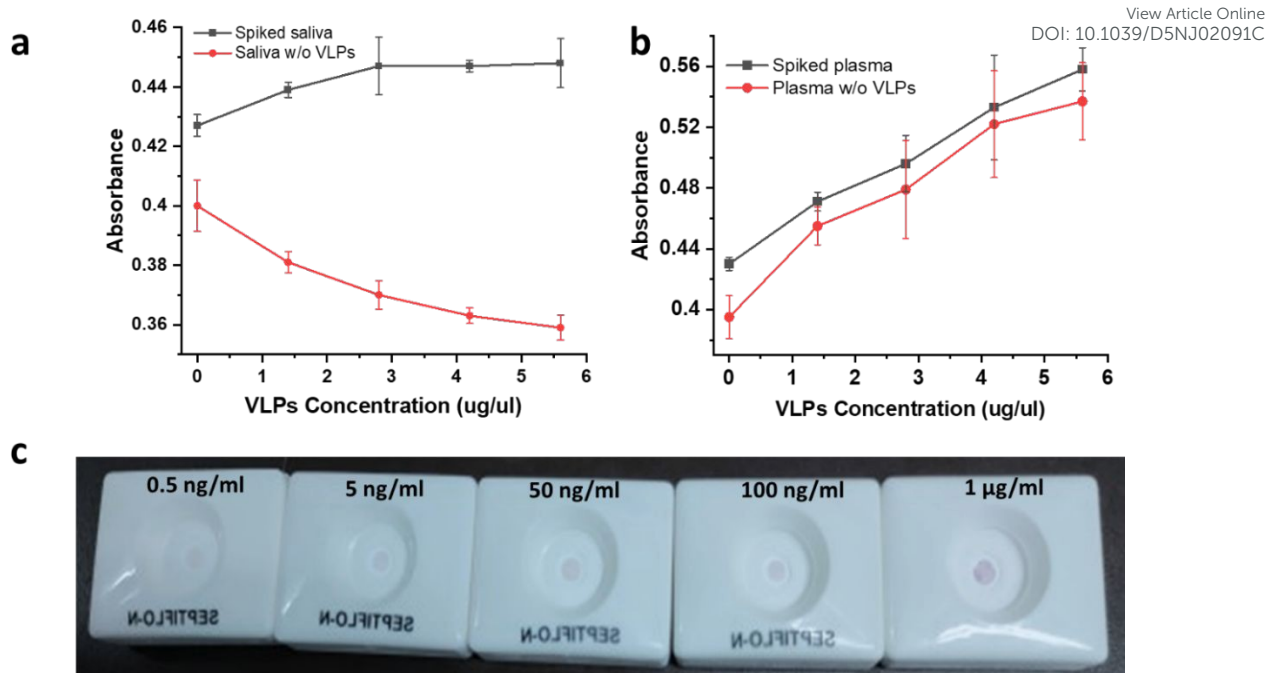


Figure 5: Comparative analysis of the interaction of synthesized AuNP-ACE2-2 particles in two different biological matrices, namely, (a) saliva and (b) plasma, and (c) gradient developed in flow-through assay for saliva samples.

Clinical Utility and Performance Validation: A distinguishing feature of our bioassay is its potential applicability in both point-of-care (POC) bedside testing and large-scale screening programs. To evaluate this capability, we conducted a comparative analysis between our developed assay and a commercially available saliva-based diagnostic kit. The study involved testing saliva samples spiked with virus-like particles (VLPs) alongside the standard control solutions provided with the commercial kit, using both platforms- the developed assay and the marketed kit. The results obtained for the spiked saliva samples demonstrated high consistency and comparability between both the systems (**Fig. 6a**). This was confirmed by running a t-test across the two assays; the p-value was found to be 0.53. This obtained value implies that there is no significant difference in the performance of the two assays at the confidence interval of 95% (**Fig. 6b**). Further, we observed that the in-house assay could outperform the marketed kit at a lower concentration, implying higher sensitivity and potential in the market. Sensitivity and specificity were assessed using 30 aliquoted healthy saliva samples spiked with varying viral loads and 20 controls (**Fig. S4**). The assay achieved a sensitivity of 96.67% and specificity of 95%, with a limit of detection (LOD) of 0.02 pg/ μ l. Comparative analysis with a marketed SARS-CoV-2 detection kit demonstrated the superior performance of our assay. The receiver operating characteristic (ROC) curve analysis yielded an area under the curve (AUC) of 0.997

($p < 0.001$), indicating excellent diagnostic accuracy (**Fig. 6c**). Notably, the developed assay exhibited a remarkable correlation with the performance of the commercial kit, exceeding our initial expectations.

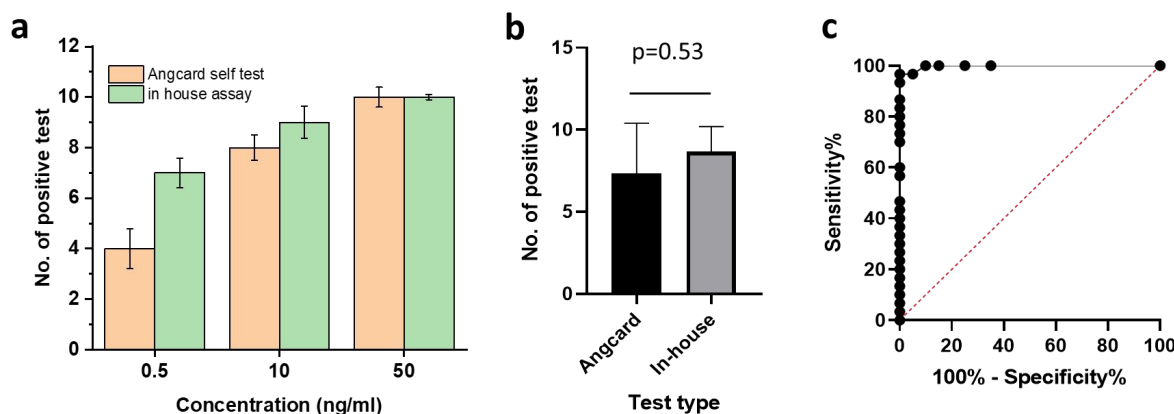


Figure 6: (a) Comparative analysis of the performance of marketed kit and inhouse developed flow-through assay in saliva spiked with varying concentrations and (b) t-test test confirming there is no significant difference in the performance of marketed kit and our flow-through assay (p -value is 0.53) and (c) ROC analysis of flow-through assay.

Discussion:

The study aimed to evaluate the suitability of different biological matrices for SARS-CoV-2 detection with a particular focus on saliva as an alternative to nasopharyngeal swabs. The decision to use saliva was supported by evidence that at certain stages of infection, nasopharyngeal swabs may yield false negatives while saliva samples consistently provide positive results. This observation aligns with previous findings where saliva tested positive in patients whose respiratory tract specimens were negative for SARS-CoV-2, suggesting viral shedding through saliva can persist even when nasopharyngeal samples appear clear³². This serves as a merit for our developed flow-through assay. Furthermore, the viral load in saliva is reported to range from 9.9×10^2 to 1.2×10^8 copies/mL, implying a strong potential for its use as a diagnostic matrix³³. A crucial limitation of existing RT-PCR-based methods is their reliance on nucleic acid detection, which may lead to prolonged positive results even after the infectious virus has been cleared^{34, 35}. Our approach circumvented this issue by targeting viral proteins instead of RNA, ensuring that the detection was specific to the presence of active viral components. The studies reported in **Table 1** provide a unique approach to the diagnosis of SARS-CoV-2, reflecting their exclusivity and comparability to the developed assay reported

1
2
3 in this paper. Additionally, the use of gold nanoparticles (AuNPs) in the reported assay View Article Online
DOI: 10.1039/D3NJ02091C
4 conferred several advantages, including low toxicity ³⁶, ease of synthesis ³⁷, a visual signal ¹⁹,
5 and functionalization capabilities ³⁸. The characterization of the synthesized nanoparticles
6 confirmed a monodisperse distribution, and the observed redshift and increase in
7 hydrodynamic diameter validate the successful binding of ACE2 on the gold surface in **Fig.**
8 **2a, b**. The decrease in zeta potential upon PEGylation, as well as the increase in surface
9 potential due to the positively charged domain of the receptor, further confirmed the stability
10 and functionality of our nanoconjugates (**Fig. 2c, e**)^{39, 40}.

11
12 For efficient antigen detection, the development of both capture and detection probes is
13 typically required. However, the urgent need for rapid diagnostic tools during the pandemic
14 necessitated an alternative approach. To bypass the constraints of developing two antibody
15 pairs, we utilized ACE2, the natural receptor for the SARS-CoV-2 spike protein as the capture
16 probe. In earlier reported studies, ACE2 demonstrated a high binding affinity for the viral
17 antigen, with KD values of 319.7 nM for S1 and 13.18 nM for the receptor-binding domain
18 (RBD) ⁴¹. Previous studies have established that the proteolytically activated S protein of
19 SARS-CoV-2 binds to ACE2 with a higher affinity than its SARS-CoV counterpart ⁴²,
20 reinforcing the reliability of ACE2 as a capture agent. Our results demonstrated successful
21 sandwich detection of the S1 antigen using ACE2, confirming and making it a robust
22 alternative to traditional antibody-based assays.

23
24 The superior performance of our AuNP-ACE2-2 assay in saliva compared to plasma can be
25 attributed to the distinct physicochemical properties of the two matrices. Plasma contains a
26 complex mixture of proteins, predominantly high-molecular-weight proteins like albumin,
27 globulins, and fibrinogen (~50–70 mg/mL) that can strongly adsorb onto the gold nanoparticle
28 (AuNP) surface, forming a dense protein corona. This phenomenon can mask functional
29 surface ligands (e.g., ACE2), sterically hinder target binding, and lead to aggregation or altered
30 particle behavior, ultimately reducing assay sensitivity and increasing background noise ^{43,44}
31 Saliva, in contrast, contains a lower total protein concentration (~0.7–2.4 mg/mL) and a
32 different proteomic profile with fewer high-affinity corona-forming proteins ⁴⁵. This minimizes
33 nonspecific adsorption, leading to a weakly bound corona layer. As demonstrated by Grewal
34 et al. (2023), gold nanoparticle-based biosensors show greater stability and reduced
35 interference in saliva due to the lower presence of thiol- or amine-rich proteins and mucins that
36 compete for nanoparticle surface binding⁴⁶. Furthermore, the reduced ionic strength and lower
37
38
39
40
41
42
43
44
45
46
47
48
49
50
51
52
53
54
55
56
57
58
59
60

viscosity of saliva support better nanoparticle dispersion and reduce aggregation risk – critical factors for optical signal reliability in colorimetric or plasmonic assays.

The enhanced assay sensitivity and specificity observed in saliva (as supported by **Fig. 5b**) likely stem from these favourable interactions, allowing the AuNP-ACE2-2 complex to maintain its active conformation and interact more effectively with its viral targets. Additionally, the lower autofluorescence and absorbance background of saliva contribute to improved signal-to-noise ratios, a key advantage for point-of-care or field-deployable diagnostic systems⁴⁷. The viral load in saliva was found to be within the range of 0.1 ng/ μ L to 1 μ g/ μ L, which facilitated the development of a color gradient-based detection system. The generated color chart enables semi-quantitative estimation of viral load, allowing individuals to infer the progression of their infection (**Fig. S5**). For instance, a light pink spot corresponding to chart 1 suggests early-stage infection, while a darker hue matching chart 3 or 4 indicates later-stage viral shedding³³. This approach provides a user-friendly method for tracking infection dynamics, enabling individuals to determine when to self-isolate and seek medical attention based on persistent high viral loads. This approach ensures broad accessibility, especially in low-resource or point-of-care settings where affordability and ease of interpretation are critical parameters. The high performance of our assay compared to commercial counterparts underscores its potential for widespread application in point-of-care diagnostics.

By enabling early and continuous detection of the virus, our assay has the potential to improve isolation strategies and curb transmission. The combination of saliva-based detection, ACE2 capture probes, and a visual color-based readout enhances user-friendliness, particularly for individuals in quarantine settings. Though slightly lower in absolute sensitivity and specificity than lab-based methods, the assay achieves strong discrimination in raw saliva. As shown in **Fig. 6**, its performance aligns with rapid antigen tests, offering faster turnaround, simplicity, and sample flexibility.

Table 1: A comparative study of saliva-based and recombinant antigen protein-based detection techniques.

Sr · N o.	Method	Target	LOD	Chemistry	Clinical samples & validatio n	Refere nce

1.	electrochemical	RNA (NPS & Saliva)	6.9 copies/ μ L	Graphene sheet+ oligos	22 covid patients+ 26 healthy	<u>10</u>
2.	CASSPIT (Cas13 Assisted Saliva-based & Smartphone Integrated Testing)	RNA	~200 copies	RNA reporter molecule conjugated with 6-carboxyfluorescein (FAM)	96 covid patients	<u>8</u>
3.	RT-LAMP	RNA	304 viral copies	LAMP reaction mix+SYBR green	20 samples	<u>11</u>
4.	LFA rapid-antigen	Spike protein	472 copies/ μ l	Polyclonal Ab (sensitive-93%)	122 patients	<u>12</u>
5.	SERS	Spike Protein	4 pg/mL	AuNp+anti-spike Ab	No	<u>13</u>
6.	Microfluidic	Spike protein	1fg/ml-10 μ g/ml 100-2500 PFU/ml	Gold electrodes coated with Ab	No	<u>14</u>
7.	Multiplex bead-based immunoassay	IgG	NA	SARS-CoV-1 antigen +magnetic microparticles	33 covid patients	<u>15</u>
8.	Electrochemical (EIS) Square Wave Voltammetry (SWV)	Nucleocapsid protein	0.2 nM 0.4 nM	MIP-polypyrrole + AuNP-modified SPE	Recombinant nucleocapsid	48
9.	Electrochemical	Nucleocapsid protein	51.2 \pm 2.8 pg/mL	Molecularly imprinted composite polymer system	Recombinant nucleocapsid	49
10.	Evaluation study (MIP polypyrrole)	Spike protein	-	Molecularly imprinted polypyrrole (MIP-Ppy) and non-imprinted polypyrrole (NIP-Ppy)	Recombinant spike protein	50
11.	Electrochemical	Spike glycoprotein	-	MIP-based sensor	Recombinant spike protein	51

View Article Online
DOI: 10.1039/D5NJ02091C

12	Electrochemical	Infectious disease biomarkers	-	MIP-based electrochemical platforms	-	DOI: 10.1039/D5NJ02091C
	Our work	S1 protein	0.02 pg/ μ l	AuNp-ACE2+S1 protein	Self-collected spiked saliva	

Given its superior performance compared to commercial kits (**Fig. 6**), this assay holds significant promise for large-scale diagnostic applications, particularly in resource-limited settings. Future work may focus on further refining the assay's detection limits exploring its applicability to emerging viral variants, and integrating it into broader public health surveillance strategies. While SARS-CoV-2 and other coronaviruses are well-known for their spike (S) proteins, several other respiratory viruses also have spike-like surface proteins that mediate host cell entry. Although we have targeted the SARS-CoV-2 virus specifically in this study, a less complicated design of the developed flow-through assay can enable the detection of multiple viruses like SARS-CoV-1 and HCoV-NL63 due to shared ACE2-binding motifs⁵³. This can be addressed as a future scope to build a multi-detection platform in a single cassette of respiratory viruses. Although previous studies have confirmed the high binding specificity between SARS-CoV-2 spike protein and ACE2, with significantly lower or no affinity observed for other viruses, cross-reactivity testing is a crucial step for clinical translation, which is to be included in the study while clinical testing with real samples.

Conclusion:

This study presents the synthesis of specialized particles and the development of a feasible system for a saliva-based, single-step flow-through assay. The results demonstrate that the proposed system effectively differentiates SARS-CoV-2-infected individuals from healthy, uninfected subjects, highlighting its potential for accurate SARS-CoV-2 diagnosis. Compared to commercially available saliva-based detection techniques, the in-house-developed flow-through assay offers several significant advantages, including a rapid analysis time of approximately 10 minutes, minimal sample preparation without the need for RNA extraction, reverse transcription, or thermal cycling, and the use of cost-effective equipment. Additionally, the assay exhibits high diagnostic performance, with sensitivity and specificity values of 96.67% and 95%, respectively, supporting its potential for commercialization. The limit of detection (LOD) of 0.02 pg/ μ l of the developed assay is comparable to other established

methods in the literature. Given these advantages, this flow-through assay represents a promising tool for public health applications, as its implementation could enhance SARS-CoV-2 detection capacity and contribute to efforts aimed at controlling the severe reoccurrence of COVID-19.

Data availability

The data supporting this article have been included as part of the ESI.

Conflicts of interest

There are no conflicts of interest to declare.

Acknowledgements

The authors thank the funding agencies, Science and Engineering Research Board, DST for the grant (SRG/2023/001099), and CSIR-ASPIRE grant (01WS (009)/2023-24/EMR-II/ASPIRE). The authors also thank Central Research Facility (CRF) of Indian Institute of Technology Delhi for extensive use of TEM facility.

References

- 1 Z. Abduljaleel, *Biophys. Chem.*, 2025, **320–321**, 107413.
- 2 F. Tian, B. Tong, L. Sun, S. Shi, B. Zheng, Z. Wang, X. Dong and P. Zheng, *eLife*, 2021, **10**, e69091.
- 3 N. Z. Zabidi, H. L. Liew, I. A. Farouk, A. Puniyamurti, A. J. W. Yip, V. N. Wijesinghe, Z. Y. Low, J. W. Tang, V. T. K. Chow and S. K. Lal, *Viruses*, 2023, **15**, 944.
- 4 P. Laine, H. Nihtilä, E. Mustanoja, A. Lyyski, A. Ylinen, J. Hurme, L. Paulin, S. Jokiranta, P. Auvinen and T. Meri, *J. Med. Virol.*, 2022, **94**, 1227–1231.
- 5 L. Rivett, S. Sridhar, D. Sparkes, M. Routledge, N. K. Jones, S. Forrest, J. Young, J. Pereira-Dias, W. L. Hamilton, M. Ferris, M. E. Torok, L. Meredith, The CITIID-NIHR COVID-19 BioResource Collaboration, R. Gupta, P. A. Lyons, M. Toshner, B. Warne, J. Bartholdson Scott, C. Cormie, H. Gill, I. Kean, M. Maes, N. Reynolds, M. Wantoch, S. Caddy, L. Caller, T. Feltwell, G. Hall, M. Hosmillo, C. Houldcroft, A. Jahun, F. Khokhar, A. Yakovleva, H. Butcher, D. Caputo, D. Clapham-Riley, H. Dolling, A. Furlong, B. Graves, E. L. Gresley, N. Kingston, S. Papadia, H. Stark, K. E. Stirrups, J. Webster, J. Calder, J. Harris, S. Hewitt, J. Kennet, A. Meadows, R. Rastall, C. O. Brien, J. Price, C. Publico, J. Rowlands, V. Ruffolo, H. Tordesillas, K. Brookes, L. Canna, I. Cruz, K. Dempsey, A. Elmer, N. Escoffery, H. Jones, C. Ribeiro, C. Saunders, A. Wright, R. Nyagumbo, A. Roberts, A. Bucke, S. Hargreaves, D. Johnson, A. Narcorda, D. Read, C. Sparke, L. Warboys, K. Lagadu, L. Mactavous, T. Gould, T. Raine, C. Mather, N. Ramenatte, A.-L. Vallier, M. Kasanicki, P.-J. Eames, C. McNicholas, L. Thake, N. Bartholomew, N. Brown, S. Parmar, H. Zhang, A. Bowring, G. Martell, N. Quinnell, J. Wright, H. Murphy, B. J. Dunmore, E. Legchenko, S. Gräf, C. Huang, J. Hodgson, K. Hunter, J. Martin, F. Mescia, C. O'Donnell, L. Pointon, J. Shih, R. Sutcliffe, T. Tilly, Z. Tong, C. Treacy, J. Wood, L. Bergamaschi, A. Betancourt, G. Bowyer, A. De Sa, M. Epping, A. Hinch, O. Huhn, I. Jarvis, D. Lewis, J. Marsden, S. McCallum, F. Nice, M. D. Curran, S. Fuller, A. Chaudhry, A. Shaw, R. J. Samworth, J. R. Bradley, G. Dougan, K. G. Smith, P. J. Lehner, N. J. Matheson, G. Wright, I. G. Goodfellow, S. Baker and M. P. Weekes, *eLife*, 2020, **9**, e58728.

- 1
2
3
4
5
6
7
8
9
10
11
12
13
14
15
16
17
18
19
20
21
22
23
24
25
26
27
28
29
30
31
32
33
34
35
36
37
38
39
40
41
42
43
44
45
46
47
48
49
50
51
52
53
54
55
56
57
58
59
60
- 6 M. Zhao, Y. Xu, D. Zhang, G. Li, H. Gao, X. Zeng, Y. Tie, Y. Wu, E. Dai and Z. Feng, *Virology*, 2022, **19**, 67. View Article Online
DOI: 10.1039/D5NJ02091C
- 7 M. F. Abasiyanik, B. Flood, J. Lin, S. Ozcan, S. J. Rouhani, A. Pyzer, J. Trujillo, C. Zhen, P. Wu, S. Jumic, A. Wang, T. F. Gajewski, P. Wang, M. Hartley, B. Ameti, R. Niemiec, M. Fernando, V. Mishra, P. Savage, B. Aydogan, C. Bethel, S. Matushek, K. G. Beavis, N. Agrawal, J. Segal, S. Tay and E. Izumchenko, *Sci. Rep.*, 2021, **11**, 12425.
- 8 I. Azmi, M. I. Faizan, R. Kumar, S. Raj Yadav, N. Chaudhary, D. Kumar Singh, R. Butola, A. Ganotra, G. Datt Joshi, G. Deep Jhingan, J. Iqbal, M. C. Joshi and T. Ahmad, *Front. Cell. Infect. Microbiol.*, 2021, **11**, 632646.
- 9 Y. Wang, A. Upadhyay, S. Pillai, P. Khayambashi and S. D. Tran, *Oral Dis.*, 2022, **28**, 2362–2390.
- 10 M. Alafeef, K. Dighe, P. Moitra and D. Pan, *ACS Nano*, 2020, **14**, 17028–17045.
- 11 L. E. Lamb, S. N. Bartolone, E. Ward and M. B. Chancellor, *PLOS ONE*, 2020, **15**, e0234682.
- 12 L. Azzi, A. Baj, T. Alberio, M. Lualdi, G. Veronesi, G. Carcano, W. Ageno, C. Gambarini, L. Maffioli, S. D. Saverio, D. D. Gasperina, A. P. Genoni, E. Premi, S. Donati, C. Azzolini, A. M. Grandi, F. Dentali, F. Tangianu, F. Sessa, V. Maurino, L. Tettamanti, C. Siracusa, A. Vigezzi, E. Monti, V. Iori, D. Iovino, G. Ietto, P. A. Grossi, A. Tagliabue and M. Fasano, *J. Infect.*, 2020, **81**, e75–e78.
- 13 A. Pramanik, Y. Gao, S. Patibandla, D. Mitra, M. G. McCandless, L. A. Fassero, K. Gates, R. Tandon and P. Chandra Ray, *Nanoscale Adv.*, 2021, **3**, 1588–1596.
- 14 M. Xian, H. Luo, X. Xia, C. Fares, P. H. Carey, C.-W. Chiu, F. Ren, S.-S. Shan, Y.-T. Liao, S.-M. Hsu, J. F. Esquivel-Upshaw, C.-W. Chang, J. Lin, S. C. Ghivizzani and S. J. Pearton, *J. Vac. Sci. Technol. B Nanotechnol. Microelectron. Mater. Process. Meas. Phenom.*, 2021, **39**, 033202.
- 15 N. Pisanic, P. R. Randad, K. Kruczynski, Y. C. Manabe, D. L. Thomas, A. Pecosz, S. L. Klein, M. J. Betenbaugh, W. A. Clarke, O. Laeyendecker, P. P. Caturegli, H. B. Larman, B. Detrick, J. K. Fairley, A. C. Sherman, N. Roupheal, S. Edupuganti, D. A. Granger, S. W. Granger, M. H. Collins and C. D. Heaney, *J. Clin. Microbiol.*, 2020, **59**, e02204-20.
- 16 Y. H. Chung, V. Beiss, S. N. Fiering and N. F. Steinmetz, *ACS Nano*, 2020, **14**, 12522–12537.
- 17 M. Janik, T. Gabler, M. Koba, M. Panasiuk, Y. Dashkevich, T. Łęga, A. Dąbrowska, A. Naskalska, S. Żołędowska, D. Nidzworski, K. Pyrc, B. Gromadzka and M. Śmietana, *Sci. Rep.*, 2023, **13**, 1512.
- 18 W. Andrzejewska, B. Peplińska, J. Litowczenko, P. Obstarczyk, J. Olesiak-Bańska, S. Jurga and M. Lewandowski, *ACS Synth. Biol.*, 2023, **12**, 2320–2328.
- 19 A. Karnwal, R. S. Kumar Sachan, I. Devgon, J. Devgon, G. Pant, M. Panchpuri, A. Ahmad, M. B. Alshammari, K. Hossain and G. Kumar, *ACS Omega*, 2024, **9**, 29966–29982.
- 20 A. Sena-Torralba, R. Álvarez-Diduk, C. Parolo, A. Piper and A. Merkoçi, *Chem. Rev.*, 2022, **122**, 14881–14910.
- 21 G. Liu and J. F. Rusling, *ACS Sens.*, 2021, **6**, 593–612.
- 22 V. Maya, J. E. Kaviyil, D. K. Ponnambath, R. P. Nair, A. Bhatt, R. Pilankatta, L. Valliyot, R. Ddungdung, R. A. Veettil and M. Gopi, *VirusDisease*, 2021, **32**, 78–84.
- 23 N. P. Dalva-Baird, W. M. Alobuia, E. Bendavid and J. Bhattacharya, *Eur. J. Clin. Invest.*, 2021, **51**, e13669.
- 24 A. Slomski, *JAMA*, 2022, **328**, 700.
- 25 P. Jagtap, R. Singh, K. Deepika, V. Sritharan and S. Gupta, *J. Clin. Microbiol.*, 2018, **56**, e00408-18.
- 26 F. L. Heredia, P. J. Resto and E. I. Parés-Matos, *Biosensors*, 2020, **10**, 99.
- 27 J. P. Oliveira, A. R. Prado, W. J. Keijok, P. W. P. Antunes, E. R. Yapuchura and M. C. C. Guimarães, *Sci. Rep.*, 2019, **9**, 13859.
- 28 P. Prasad, R. Singh, S. Kamaraju, V. Sritharan and S. Gupta, *ACS Appl. Bio Mater.*, 2020, **3**, 6688–6696.
- 29 J.-H. Lee, M. Choi, Y. Jung, S. K. Lee, C.-S. Lee, J. Kim, J. Kim, N. H. Kim, B.-T. Kim and H. G. Kim, *Biosens. Bioelectron.*, 2021, **171**, 112715.
- 30 J. Lan, J. Ge, J. Yu, S. Shan, H. Zhou, S. Fan, Q. Zhang, X. Shi, Q. Wang, L. Zhang and X. Wang, *Nature*, 2020, **581**, 215–220.

- 1
2
3
4
5
6
7
8
9
10
11
12
13
14
15
16
17
18
19
20
21
22
23
24
25
26
27
28
29
30
31
32
33
34
35
36
37
38
39
40
41
42
43
44
45
46
47
48
49
50
51
52
53
54
55
56
57
58
59
60
- 31 A. Mehregan, S. Pérez-Conesa, Y. Zhuang, A. Elbahnsi, D. Pasini, E. Lindahl, R. J. Howard, C. Ulens and L. Delemotte, *Biochim. Biophys. Acta BBA - Biomembr.*, 2022, **1864**, 183994. View Article Online
DOI: 10.1039/D5NJ02091C
- 32 J. Zhu, J. Guo, Y. Xu and X. Chen, *J. Infect.*, 2020, **81**, e48–e50.
- 33 Y. Pan, D. Zhang, P. Yang, L. L. M. Poon and Q. Wang, *Lancet Infect. Dis.*, 2020, **20**, 411–412.
- 34 T.-B. Kandetu, E. J. Dziuban, K. Sikuvi, R. S. Beard, R. Nghihepa, G. Van Rooyen, A. Shiningavamwe and I. Katjitae, *Disaster Med. Public Health Prep.*, 2022, **16**, 878–879.
- 35 J. Yuan, S. Kou, Y. Liang, J. Zeng, Y. Pan and L. Liu, *Clin. Infect. Dis.*, 2020, **71**, 2230–2232.
- 36 A. M. Alkilany and C. J. Murphy, *J. Nanoparticle Res.*, 2010, **12**, 2313–2333.
- 37 Y.-C. Yeh, B. Creran and V. M. Rotello, *Nanoscale*, 2012, **4**, 1871–1880.
- 38 S. J. Amina and B. Guo, *Int. J. Nanomedicine*, 2020, **Volume 15**, 9823–9857.
- 39 Y. Khaniani, Y. Ma, M. Ghadiri, J. Zeng, D. Wishart, S. Babiuk, C. Charlton, J. N. Kanji and J. Chen, *Sci. Rep.*, 2022, **12**, 12850.
- 40 R. T. Busch, F. Karim, J. Weis, Y. Sun, C. Zhao and E. S. Vasquez, *ACS Omega*, 2019, **4**, 15269–15279.
- 41 Q. Wang, Y. Zhang, L. Wu, S. Niu, C. Song, Z. Zhang, G. Lu, C. Qiao, Y. Hu, K.-Y. Yuen, Q. Wang, H. Zhou, J. Yan and J. Qi, *Cell*, 2020, **181**, 894–904.e9.
- 42 J. Shang, G. Ye, K. Shi, Y. Wan, C. Luo, H. Aihara, Q. Geng, A. Auerbach and F. Li, *Nature*, 2020, **581**, 221–224.
- 43 T. Cedervall, I. Lynch, S. Lindman, T. Berggård, E. Thulin, H. Nilsson, K. A. Dawson and S. Linse, *Proc. Natl. Acad. Sci.*, 2007, **104**, 2050–2055.
- 44 C. Zhu, G. Yang, H. Li, D. Du and Y. Lin, *Anal. Chem.*, 2015, **87**, 230–249.
- 45 D. Belstrøm, R. R. Jersie-Christensen, D. Lyon, C. Damgaard, L. J. Jensen, P. Holmstrup and J. V. Olsen, *PeerJ*, 2016, **4**, e2433.
- 46 A. Sen, H. Poulsen, S. Sondhauss and J. M. Hodgkiss, *ACS Sens.*, 2023, **8**, 1841–1849.
- 47 Y. Li, Y. Ou, K. Fan and G. Liu, *Theranostics*, 2024, **14**, 6969–6990.
- 48 V. Liustrovaite, V. Ratautaite, A. Ramanaviciene and A. Ramanavicius, *Biosens. Bioelectron.*, 2025, **272**, 117092.
- 49 M. Drobysh, V. Ratautaite, E. Brazys, A. Ramanaviciene and A. Ramanavicius, *Biosens. Bioelectron.*, 2024, **251**, 116043.
- 50 V. Ratautaite, R. Boguzaitė, E. Brazys, D. Plausinaitis, S. Ramanavicius, U. Samukaite-Bubniene, M. Bechelany and A. Ramanavicius, *Talanta*, 2023, **253**, 123981.
- 51 V. Ratautaite, R. Boguzaitė, E. Brazys, A. Ramanaviciene, E. Ciplys, M. Juozapaitis, R. Slibinskas, M. Bechelany and A. Ramanavicius, *Electrochimica Acta*, 2022, **403**, 139581.
- 52 G. Pilvenyte, V. Ratautaite, R. Boguzaitė, S. Ramanavicius, C.-F. Chen, R. Viter and A. Ramanavicius, *Biosensors*, 2023, **13**, 620.
- 53 W. Li, J. Sui, I.-C. Huang, J. H. Kuhn, S. R. Radoshitzky, W. A. Marasco, H. Choe and M. Farzan, *Virology*, 2007, **367**, 367–374.

Data Availability Statement

View Article Online
DOI: 10.1039/D5NJ02091C

The data supporting this article have been included as part of the Supplementary Information.

1
2
3
4
5
6
7
8
9
10
11
12
13
14
15
16
17
18
19
20
21
22
23
24
25
26
27
28
29
30
31
32
33
34
35
36
37
38
39
40
41
42
43
44
45
46
47
48
49
50
51
52
53
54
55
56
57
58
59
60